

FEEDBACK BOUNDARY OF 4:1 ROUNDED CONTRACTION SLIP FLOW FOR OLDROYD-B FLUID BY FINITE ELEMENT

NAWALAX THONGJUB

Department of Mathematics and Statistics, Faculty of Science and Technology,
Thammasat University, Pathumthani 12120, Thailand
E-mail: t_nawalax@hotmail.com

Abstract

The driven force feedback in viscoelastic flow is a technique to enforce converged solution of Oldroyd-B fluid on the basis of semi-implicit Taylor-Galerkin finite element method for 4:1 contraction geometry with rounded corner meshes. Meanwhile in the numerical computation, the Phan-Thien slip rule is applied to complete the slip velocity along the die wall. After application of the slip condition, the severe stress near die exit and the vortex size around contraction corner are clearly reduced. This simulation is modeled with the Navier-Stokes and Oldroyd-B equations in two-dimensional planar isothermal incompressible creeping flow. The non-linear differential models are discretised to system of linear equations with semi-implicit Taylor-Galerkin finite element method. In addition, the Streamline-Upwind/Petrov-Galerkin and velocity gradient recovery are accuracy and the stability schemes to stabilize an approximate solution. The optimal slip velocity is modified step by step by critical slip coefficient to set the slip condition at the wall and when the solutions of slip and no-slip cases are compared with analytic solution, the outcome of slip condition shows better conformity to real results.

Keywords: Feedback, Slip effect, 4:1 contraction flow, Oldroyd-B fluid, Slip velocity.

1. Introduction

This research is focused on feedback boundary of 4:1 rounded contraction slip flow for the Oldroyd-B fluid by a semi-implicit Taylor-Galerkin pressure-correction finite element method (STGFEM) under two-dimensional planar system. The kinematic behaviors of this viscoelastic fluid are strong elongation

Nomenclatures

(Non-dimensional system)

\tilde{D}	Deformation tensor rate
Π	Second invariant
Π_{crit}	Critical second invariant
Π_w	Second invariant at the wall
L	Characteristic length
n	Time step
$n + 1/2$	Half time step
$n + 1$	Full time step
\bar{P}	Pressure
n	Time step
Re	Reynolds number
t	Time
\bar{U}	Velocity
U_{mean}	Mean velocity of flowrate for no slip
U_{slip}	Slip velocity
V	Characteristic velocity
We	Weissenberg number

Greek Symbols

(Non-dimensional system)

ρ	Density
η	Viscosity
η_0	Zero-shear viscosity
η_p	Polymeric viscosity
η_s	Solvent viscosity
$\tilde{\tau}$	Polymeric component of the extra-stress tensor
λ_1	Relaxation time
τ_{xy}	Shear stress
$\dot{\gamma}$	Shear rate
α	Slip coefficient

Abbreviations

FEM	Finite Element Method
J&S	Johnson, M.W. and Segalman, D. [13]
STGFEM	Semi-implicit Taylor-Galerkin Pressure-correction Finite Element Method

and violent shear stress when the flow confronts contraction section abruptly then the streamline path suddenly changes trajectory. For this phenomenon, the slip velocity at contraction wall is calculated in order to reduce shear stress at sharp corner.

In experimental observation for viscoelastic fluids [1], the Rheogoniometer was used to measure the rheological properties in an abrupt 2 to 1 contraction domain. The significant comparison was emphasized the difference between the accomplishment result and numerical prediction of power-law model. The equipment [2] for planar contraction flows was implemented for Boger fluid. After acute numerical solution was revealed, a circular contraction flow for both Newtonian and Non-Newtonian fluids [3] has been set up to benchmark with experimental result.

To avoid inconvenient calculation from analytical data, the mathematical model of viscoelastic problem is simulated in form of non-linear partial differential equations under conservation law of mass and momentum. In this case, a complex problem is eliminated by means of numerical techniques such as finite element method, finite volume method and finite difference method. Recently, the semi-Lagrangian finite volume method [4] was applied for solving a 4:1 planar contraction of creeping flow via Oldroyd-B model. The inertial flows and the consequence procedure [5] of a new condition by changing Cartesian coordinates with axisymmetric cylindrical flow were expanded with fixed grids in Eulerian methods.

A semi-implicit Taylor-Galerkin finite element method [6] has been brought to solve stick-slip flow of Oldroyd-B problem along with the modification for free surface method at die exit boundary which was determined for Die-swell flow in terms of swelling ratio as a function of relaxation time. Consequently, the Phan-Thien/Tanner fluid in complete die of pressure-tooling problem [7] has been simulated under the same STGFEM including security technique of Streamline-Upwind Petrov/Galerkin for stabilizing converging solution. To utilize finite element method and finite volume method in the same code, the new hybrid scheme of finite volume/element method [8, 9] by means of cell-vertex discretisation technique has been proposed in order to have calculated cooperative stress and flow field for Oldroyd-B and Phan-Thien/Tanner fluids with both rounded and sharp corner contraction flows.

Collecting experimental and numerical data to study fluid flows through solid wall has demonstrated that slip velocity appears on solid surface and hence reduces shear rate. To make solution look closer to real problems, a number of literatures have set up various numerical methods to estimate slip velocity [10] at the wall on free surface. For large slip speed on die wall of HDPE and LLDPE, the deformation can be noticed under surface melt fracture [11]. In addition, the analysis solutions for capillary tubes [12] have been calculated after setting the slip velocity.

In this study, the slip condition has been employed in the problem of 4:1 contraction for Oldroyd-B model under the two-dimensional planar isothermal incompressible flow. A semi-implicit Taylor-Galerkin pressure-correction finite element method has transformed Navier-Stokes equation to a system of simple linear equations and all solutions have been stabilized by means of the Streamline-Upwind Petrov/Galerkin and velocity gradient recovery techniques. The solutions of slip condition and no slip situation have been compared after optimization of the slip coefficient with rounded corner geometries.

2. Governing Equations

The governing equations are the Navier-Stokes equations in dimensionless form of the conservation of mass and momentum for viscoelastic fluid based on non-gravity and steady incompressible flow. Considering the standard values of the fluid properties, the non-dimensional system of the continuity equation (1) and Navier-Stokes equation (2) are represented as

$$\nabla \cdot \bar{\mathbf{U}} = 0 \quad (1)$$

$$\text{Re} \frac{\partial \bar{\mathbf{U}}}{\partial t} = \nabla \cdot \tilde{\mathbf{T}} - \text{Re} \bar{\mathbf{U}} \cdot \nabla \bar{\mathbf{U}} - \nabla \bar{P} \quad (2)$$

$$\text{Re} = \frac{\rho V L}{\eta_0} \quad (3)$$

The non-dimensional parameters are $\text{Re} = 0$, $\frac{\eta_p}{\eta_0} = \frac{8}{9}$, and $\frac{\eta_s}{\eta_0} = \frac{1}{9}$.

$$\tilde{\mathbf{T}} = \tilde{\boldsymbol{\tau}} + 2\eta_s \tilde{\mathbf{D}} \quad (4)$$

$$\tilde{\mathbf{D}} = \frac{\nabla \bar{\mathbf{U}} + (\nabla \bar{\mathbf{U}})^t}{2} \quad (5)$$

The non-dimensional constitutive equation of Oldroyd-B fluid is represented as

$$\text{We} \tilde{\boldsymbol{\tau}}_t = \text{We} \left[\tilde{\boldsymbol{\tau}} \cdot \nabla \bar{\mathbf{U}} + (\nabla \bar{\mathbf{U}})^t \cdot \tilde{\boldsymbol{\tau}} - \bar{\mathbf{U}} \cdot \nabla \tilde{\boldsymbol{\tau}} \right] + 2\eta_p \tilde{\mathbf{D}} - \tilde{\boldsymbol{\tau}} \quad (6)$$

$$\text{We} = \frac{\lambda_1 V}{L} \quad (7)$$

The analytical values (J&S) of the shear stress [13] of Oldroyd-B fluid is demonstrated as a function of viscosity and shear rate where a is a scalar parameter on interval $(0, 2)$ as below

$$\tau_{xy} = \eta_s \dot{\gamma} + \frac{\eta_p \dot{\gamma}}{a(2-a)(\eta_p \dot{\gamma})^2 + 1} \quad (8)$$

3. Computer Programme

A finite element method is employed to compute the non-linear differential equations as the Navier-Stokes equation and the constitutive equation of Oldroyd-B model. The governing equations are discretised to three time stages by a semi-implicit Taylor-Galerkin pressure-correction scheme. And then the derivative equations are converted to linear equations and solved by the iterative method and Cholesky decomposition scheme. The Feedback STGFEM is employed to approach the converged solution and be stabilized by the streamline-upwind Petrov/Galerkin and velocity gradient recovery techniques. For studying slip effect, Phan-Thien slip

rule is applied to compute the appropriate slip velocity at wall to reduce the severe stress at contraction geometries as detailed in previous paper [14].

3.1. Semi-implicit Taylor-Galerkin pressure-correction finite element method

Semi-implicit Taylor-Galerkin pressure-correction finite element method is the integration of time-splitting step scheme and finite element method. This method is based on a semi-implicit fractional step method to discretise non-dimensional Navier-Stokes equation (2) and constitutive equation (6) to three stages per time step.

The finite difference discretisation is used to transform the initial and boundary value problem accomplished with the partial differential equations (2) and (6). The time derivative is replaced by Taylor series and the space (spatial) term is expanded by the weight residual of Galerkin finite element method. After that the three stages per time step are converted to the system of linear equations, the approximate solution of steps 1a, 1b and 3 are computed with Jacobi iterative method whereas step 2 is calculated by Cholesky decomposition algorithm.

Step 1a:

$$\begin{aligned} & \frac{2Re}{\Delta t} (\bar{U}^{n+1/2} - \bar{U}^n) \\ & = \left[\nabla \cdot (\tilde{\tau} + 2\eta_s \tilde{D}) - Re \bar{U} \cdot \nabla \bar{U} - \bar{P} \right]^n + \nabla \cdot \eta_s (\tilde{D}^{n+1/2} - \tilde{D}^n) \end{aligned} \quad (9)$$

$$\begin{aligned} & \frac{2We}{\Delta t} (\tilde{\tau}^{n+1/2} - \tilde{\tau}^n) \\ & = \left[2\eta_p \tilde{D} - \tilde{\tau} + We (\tilde{\tau} \cdot \nabla \bar{U} + (\nabla \bar{U})^t \cdot \tilde{\tau} - \bar{U} \cdot \nabla \tilde{\tau}) \right]^n \end{aligned} \quad (10)$$

Step 1b:

$$\begin{aligned} & \frac{Re}{\Delta t} (\bar{U}^* - \bar{U}^n) \\ & = \left[\nabla \cdot (2\eta_s \tilde{D}) - \nabla \bar{P} \right]^n + \left[\nabla \cdot \tilde{\tau} - Re \bar{U} \cdot \nabla \bar{U} \right]^{n+1/2} + \nabla \cdot \eta_s (\tilde{D}^* - \tilde{D}^n) \end{aligned} \quad (11)$$

$$\begin{aligned} & \frac{We}{\Delta t} (\tilde{\tau}^{n+1} - \tilde{\tau}^n) \\ & = \left[2\eta_p \tilde{D} - \tilde{\tau} + We (\tilde{\tau} \cdot \nabla \bar{U} + (\nabla \bar{U})^t \cdot \tilde{\tau} - \bar{U} \cdot \nabla \tilde{\tau}) \right]^{n+1/2} \end{aligned} \quad (12)$$

Step 2:

$$\nabla^2 (\bar{P}^{n+1} - \bar{P}^n) = \frac{2Re}{\Delta t} \nabla \bar{U}^* \quad (13)$$

Step 3:

$$\frac{2Re}{\Delta t} (\bar{U}^{n+1} - \bar{U}^*) = - (\bar{P}^{n+1} - \bar{P}^n) \quad (14)$$

where * is the intermediate time step.

3.2. Phan-Thien slip rule

The slip effect is the phenomenon that the slip velocity occurs at wall, observed in industrial process and experiment in science. Phan-Thien slip rule [15] is effective to fit slip velocity at wall because the outcome is close to experimental result [16]. The slip velocity is expressed as a function of wall shear stress and the slip velocity will be calculated when a critical shear stress is less than the wall shear stress. The behavior of second invariant is similar to the shear rate [14], so the second invariant value is used to calculate the slip velocity as below.

$$U_{slip} = U_{mean} - U_{mean} \cdot e^{-\alpha \Pi_w / \Pi_{crit}} \quad (15)$$

3.3. The driven force feedback

To enforce the numerical solution to converged solution, feedback of pressure-driven velocity flow [17] is used to set the boundary condition at inlet each step until the inlet flow approaches steadiness. For viscoelastic fluid, this technique is effective by setting the intermediate boundary to control the approximate solution. After that the numerical result will adjust smoothly and eliminate the case of jumping to the diverged solution.

This scheme uses the differential time step at 0.1 and then differential time step will be reduced step by 0.1 when the numerical error reaches to terminate this the differential time. After that we started to set the initial column (C1) from considering the stress, pressure and velocity at nodes along C2, C3 and C4 as seen in Fig 1. Considering the values of C4, it is found that the maximum error of C4 is less than the other columns, the values nodes between 22 and 28 will be set up to instate the values of nodes 1 - 7 in C1. This concept is still operated to find the boundary condition at inlet until the numerical solution is converged. The effective use under the driven force feedback flow for velocity and pressure is developed in order to reduce the time step from the repetition of the computation and approach steadily analytical solution, as outlined in *Appendix A*.

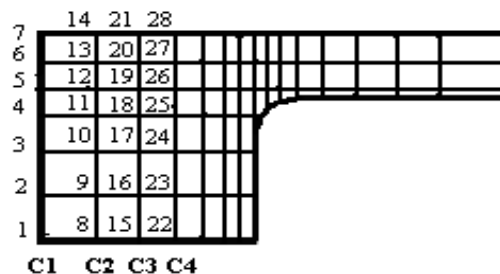


Fig. 1. Example of nodes and columns in the driven force feedback flow for the velocity and pressure.

4. Results and Discussion

The effect of 4:1 contraction problem such as shark skin phenomenon and severe stress when especially viscoelastic fluids pass the sharp corner happen clearly in engineering and industrial process. In this research, the acute geometry is curved to rounded corner in order to reduce large stress values and lip vortex by

Aboubacar et al. [8, 9]. In addition, the slip velocity is applied on the channel wall by means of Phan-Thien slip rule [14, 17].

In Fig 2(a), the symmetric geometry of planar 4:1 contraction is located at the center line. The half channel length of $4L$ and L channel widths are long enough to develop Poiseuille flow at inlet and exit sections which are $27.5L$ and $49L$, respectively.

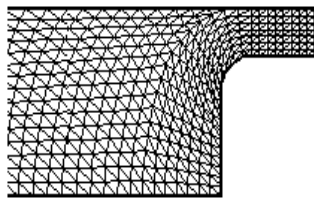
$$U_x(y) = \frac{3}{128}(16 - y^2), V_y = 0 \tag{16}$$

$$\tau_{xx} = 2Wen\eta_p \left(\frac{\partial U_x}{\partial y} \right)^2, \tau_{yy} = 0, \text{ and } \tau_{xy} = \eta_p \frac{\partial U_x}{\partial y} \tag{17}$$

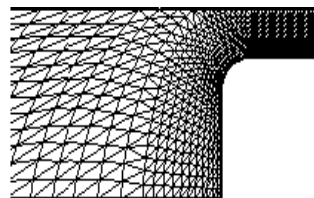
The three different patterns of coarse, medium, and fine meshes are mesh1, mesh2 and mesh3 as shown in Fig. 2(b), 2(c) and 2(d), respectively. The subdomain of every mesh is cut at position $x = 22$ to $x = 30$ from the full domain. The smallest element size of unbiased mesh structure is generated near rounded corner and the mesh specifications are defined in Table 1.



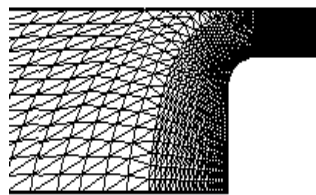
(a) the domain of mesh2



(b) mesh1



(c) mesh2



(d) mesh3

Fig. 2. Mesh patterns.

Table 1. Mesh specification of rounded corner.

	mesh1	mesh2	mesh3
Elements	1626	2693	4751
Nodes	3433	5652	9790
Degree of Freedom	18069	29740	51470
The Minimum of Mesh Size	0.017	0.010	0.006

Effect of Slip Condition Problem

The results for viscoelastic flows of rounded corner meshes under the condition of no slip and slip effect are considered and the best mesh is selected to display final solution that duplication would reduce as well as saving computer times. After the best mesh had been selected, it was applied to operate no slip case and slip condition for further details as above. A stick or no slip problem has been studied by collecting stresses and shear rate so the highest values of normal stress, shear stress and shear rate $\dot{\gamma}$ on bottom downstream wall are compared in order to choose an optimal mesh. As such, mesh2 was select as a model of final solution.

For Oldroyd-B fluids, the peak values of $\dot{\gamma}$ in Table 2 are considered with no-slip on wall for various We . The peak values on bottom downstream wall of $\dot{\gamma}$ for mesh1 vary as a function of We but in contrast to mesh2 and mesh3. As such, mesh1 is terminated by inconsistent value when compared in group. Maxima of all stresses in Table 3 look alike in mesh refinement. For this problem, the rounded corner mesh2 in a similar fashion to mesh3 is picked up for further runs because it is simple to access and the results are in close agreement with the outcome of mesh3 but the time step of mesh3 is more than the time step of mesh2 for all We values. We have selected mesh2 to simulate the slip case for reducing the calculated time.

Table 2. The peak values of $\dot{\gamma}$ on the bottom down-stream wall with no-slip.

We	mesh1	mesh2	mesh3
0.25	3.822	3.852	3.976
0.5	3.913	3.786	3.857
0.75	4.043	3.629	3.804
1	4.169	3.443	3.600

Table 3. The peak values of stresses on the bottom down-stream with no-slip at $We = 1$.

	mesh1	mesh2	mesh3
τ_{xx}	18.218	19.804	20.092
τ_{xy}	7.839	9.662	9.955
τ_{yy}	5.794	7.704	7.765

In the context of viscoelastic fluid, the peak values of normal stress $\dot{\gamma}$ on bottom downstream wall with no-slip for different values of We can be observed in Fig. 3. Since all oscillation graphs look similar in pattern but higher values of We climb up fast and drop quickly, this can be assigned to the fact that higher We values have longer relaxation time. This implies that the trend keeps higher

memory profile of its path and then its memory of original position leads to its drop in close vicinity of the beginning location.

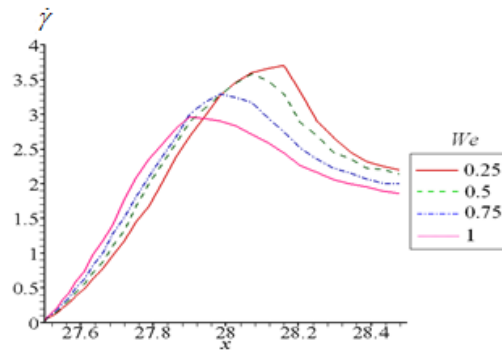


Fig. 3. $\dot{\gamma}$ on the bottom downstream wall without slip of Oldroyd-B fluid for mesh2.

To find the appropriate slip velocity, we have found the optimum slip coefficient $\alpha = 0.1$ for selecting the critical Π for all We . When we have set $\alpha = 0.1$, the highest values of shear rate along the wall are reduced. $\Pi=3.3$, $\Pi = 2.3$, $\Pi = 2.3$ and $\Pi = 2.4$ are the critical Π for $We = 0.25, 0.5, 0.75$ and 1 , respectively as illustrated in Fig 4. In addition, the shear rate line of the best of slip velocity clearly becomes lower than no-slip condition and it is given the smoothest line when it is compared with other slip velocity values.

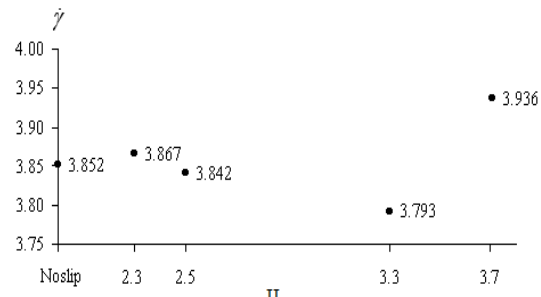
In a similar manner to sharp corner mesh, the previous algorithm is set up to imply the least shear rates of all We values and finally the critical second invariants are adjusted to the values in Table 4. This table reflects that when the critical Π is modified properly, the appropriate α is 0.1 for any values of We .

The streamline contour for $We = 1$ of mesh2 with slip at $\alpha = 0.1$ and $\Pi = 2.4$ is depicted in Fig 5. The vortex size of slip problem is smaller than no-slip as well as $We = 0.25, 0.5$ and 0.75 . There is slight alteration to a rounded corner because the stability of a rounded corner is more than a sharp corner whilst the stress value of the sharp corner is higher than that of a rounded corner at contraction.

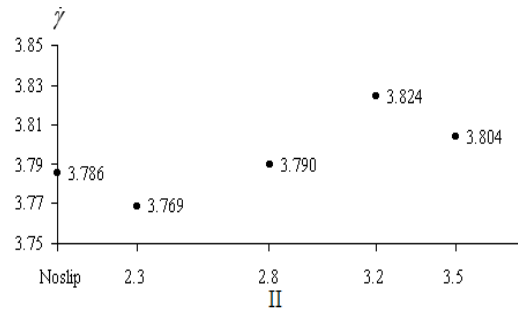
In addition, the line plot between the shear stress versus the shear rate of slip, no slip and analytical result are compared in Fig 6 and the analytical line is denoted by J&S. The solution of the slip effect that is run by mesh2, is slightly different from J&S with the percentage error 1.8295% for $We = 0.25$ and 0.0792% for $We = 1$ and it is closer to J&S more than no-slip condition with the error 8.1690% for $We = 0.25$ and 0.3984% for $We = 1$, as depicted in Fig 6. The slip condition has less approximate error than its no- slip counterpart.

Table 4. The least shear rate for proper α and suitable Π of Oldroyd-B fluid with mesh2.

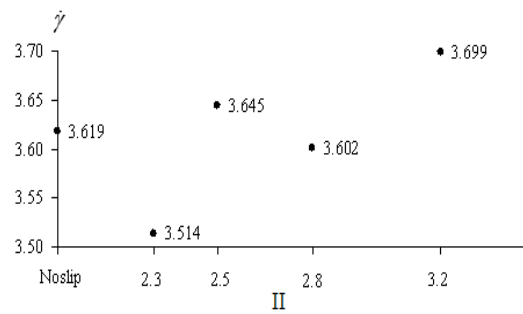
We	0.25	0.5	0.75	1
Π_{crit}	3.3	2.3	2.3	2.4
$\dot{\gamma}$	3.793	3.769	3.514	3.326
α	0.1	0.1	0.1	0.1



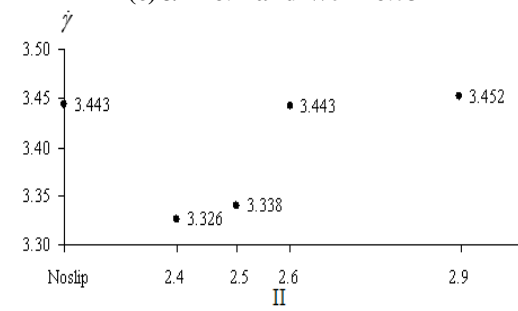
(a) $\alpha = 0.1$ and $We = 0.25$



(b) $\alpha = 0.1$ and $We = 0.5$



(c) $\alpha = 0.1$ and $We = 0.75$



(d) $\alpha = 0.1$ and $We = 1$

Fig. 4. The peak of $\dot{\gamma}$ versus Π for mesh2 along bottom downstream wall.

Comparing the appropriate slip values at the wall and without slip, we found that the slip influence can slightly reduce the peak τ_{xx} and the high shear rate $\dot{\gamma}$ as displayed in Table 5.

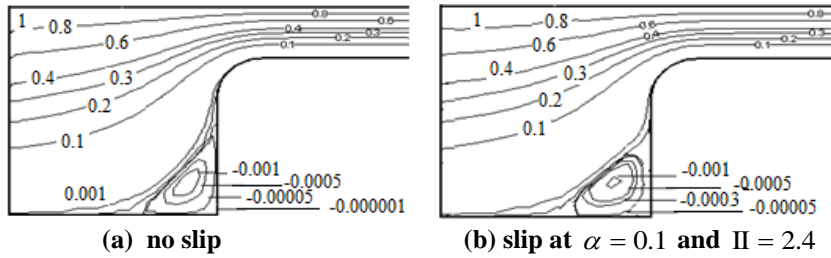


Fig. 5. Streamline contour for mesh2 along bottom downstream wall

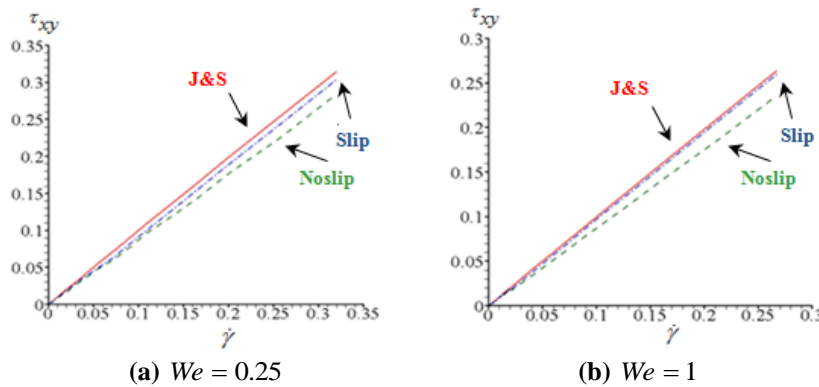


Fig. 6. The comparison of τ_{xy} versus $\dot{\gamma}$ with J&S for mesh2 on bottom downstream wall of Oldroyd-B fluid.

Table 5. The peak value of $\dot{\gamma}$ and τ_{xx} on the bottom downstream wall for mesh2.

We	$\dot{\gamma}$		τ_{xx}	
	no slip	slip	no slip	slip
0.25	3.385	3.793	5.682	5.567
0.5	3.786	3.769	11.243	11.116
0.75	3.629	3.530	15.989	15.952
1	3.443	3.326	19.804	19.659

For the no slip condition, the fluid velocity is zero at wall boundary whilst the real phenomenon makes us know that the velocity would not be zero so the slip condition is set to predict optimal velocity from the critical second invariant. Under slip situation, the stresses are reduced and jump to the analytical value (J&S) more than the no slip case, thus this effect leads the way to diminish vortex size.

The solutions of slip condition at $We = 1$ are depicted in Fig 7. The highest values of stress are located along rounded corner geometry same as sharp corner contraction. The maximum velocity in x -direction appears along symmetry line while the maximum velocity of y -direction is placed near rounded corner.

Maximum value of pressure started at inlet and then gradually decreases until it is vanished at outlet.

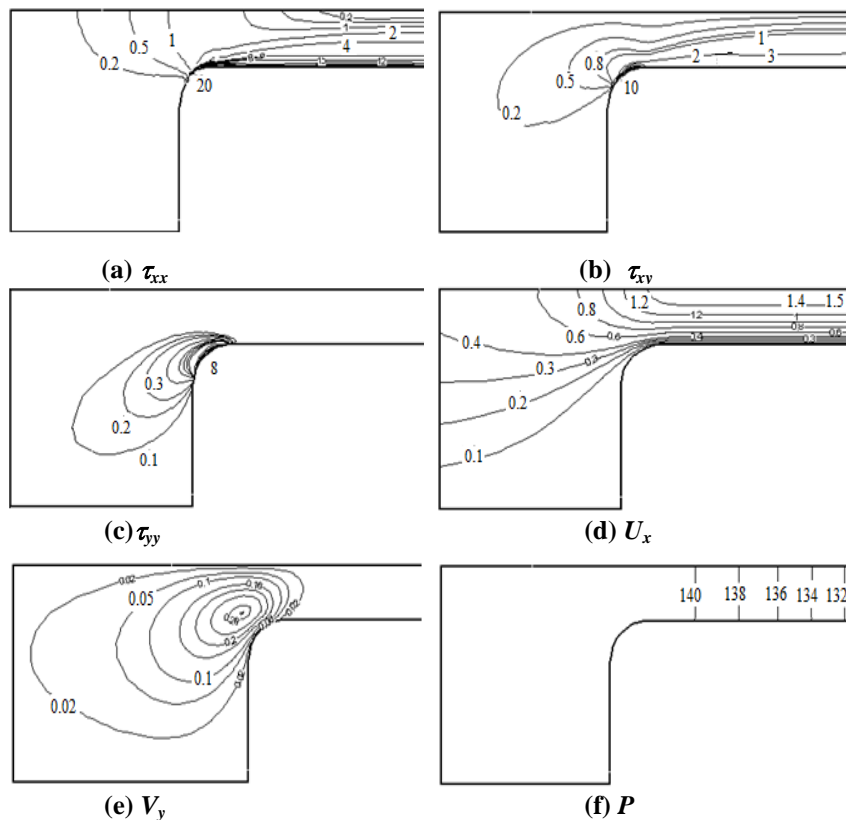


Fig. 7. Line contour with slip along channel wall at $\alpha=1$, $\Pi = 2.4$, and $We = 1$.

5. Conclusions

For steady-state viscoelastic flow in 4:1 contraction rounded geometry through planar isothermal Oldroyd-B model, the semi-implicit Taylor-Galerkin pressure-correction finite element scheme and the driven force feedback flow are employed to solve the nonlinear partial differential equation for stick before Phan-Thien slip rule is added to calculate velocity at channel wall. The streamline pattern, stress visualization and velocity field contours were depicted to compare rounded corner meshes with sharp corner meshes. All figures gave the same trend when varied Weissenberg numbers but the significant differences of vortex sizes were noticed conveniently.

After appropriate critical Π was adjusted, the slip coefficient of Viscoelastic fluids with rounded corner meshes is investigated for the optimum value of 0.1. The appropriate values of the slip coefficient and the second invariant cause the peak of shear rate lower than no-slip case and vortex size of sharp corner domain was decreased more than rounded corner shape. In case of the right selection for second invariant, this proper slip coefficient well reduces the peak of shear rate and vortex size since the velocity at wall forces fluid flow with smooth path and

stable outcome. In addition, the higher α and Π presented more oscillations that brought to the phenomenon of shark skin.

References

1. Boger, D.V.; and Ramamurthy, A.V. (1972). Flow of viscoelastic fluids through an abrupt contraction. *Rheologica Acta*, 11, 61-69.
2. Walters, K.; and Rawlinson, D.M. (1982). On some contraction flows for boger fluid. *Rheologica Acta*, 21, 547-552.
3. Boger, D.V. (1987). Viscoelastic flows through contractions. *Annual Review of Fluid Mechanics*, 19, 157-182.
4. Phillips, T.N.; and Williams, A.J. (1999). Viscoelastic flow through a planar contraction using a semi-Lagrangian finite volume method. *Journal of Non-Newtonian Fluid Mechanics*, 87, 215-246.
5. Phillips, T.N.; and Williams, A.J. (2002). Comparison of creeping and inertial flow of an oldroyd b fluid through planar and axisymmetric contractions. *Journal of Non-Newtonian Fluid Mechanics*, 108(1-3), 25-47.
6. Ngamaramvaranggul, V.; and Webster, M.F. (2001). Viscoelastic simulation of stick-slip and die-swell flows. *International Journal for Numerical Methods in Fluids*, 36, 539-595.
7. Ngamaramvaranggul, V.; and Webster, M.F. (2002). Simulation of pressure-tooling wire-coating flow with Phan-Thien/Tanner models. *International Journal for Numerical Methods in Fluids*, 38, 677-710.
8. Aboubacar, M.; and Webster, M.F. (2001). A cell-vertex finite volume/element method on triangles for abrupt contraction viscoelastic flows. *Journal of Non-Newtonian Fluid Mechanics*, 98, 83-106.
9. Aboubacar, M.; Matallah, H. and Webster, M.F. (2002). Highly elastic solutions for Oldroyd-b and Phan-Thien/Tanner fluids with a finite volume/element method: Planar contraction flows. *Journal of Non-Newtonian Fluid Mechanics*, 103, 65-103.
10. Silliman, W.J.; and Scriven, L.E. (1980). Separating flow near a static contact line: slip at a wall and shape of a free surface. *Journal of Computational Physics*, 34, 287-313.
11. Ramamurthy, A.V. (1986). Wall slip in viscous fluids and influence of materials of construction. *Journal of Rheology*, 30, 337-357.
12. Jiang, T.Q.; and Young, A.C. (1986). The rheological characterization of HPG gels: measurement of slip velocities in capillary tubes. *Rheologica Acta*, 25(4), 397-404.
13. Johnson, M.W.; and Segalman, D. (1977). A model for viscoelastic fluid behavior which allows non-affine deformation. *Journal of Non-Newtonian Fluid Mechanics*, 2, 255-270.
14. Thongjub, N.; Puangkird, B. and Ngamaramvaranggul, V. (2013). Simulation of slip effect with 4:1 contraction flow for Oldroyd-B fluid. *International Journal of Applied Science and Technology*, 6(3), 19-28.
15. Phan-Thien, N. (1988). Influence of wall slip on extrudate swell: A boundary element investigation. *Journal of Non-Newtonian Fluid Mechanics*, 26, 327-340.

16. Ngamaramvaranggul, V.; and Webster, M.F. (2000). Simulation of coating flows with slip effects. *International Journal for Numerical Methods in Fluids*, 33, 961-992.
17. Ngamaramvaranggul, V.; and Thongjub, N. (2014). Newtonian fluid through the abrupt 4:1 contraction flow of rounded corner geometry with feedback pressure-driven velocity flow. *International Journal of Information Technology and Computer Science*, 15(2), 1-10.

Appendix A

Flowchart of the Driven Force Feedback Flow

The below flowchart is set up to run the optimum solution (pressure, velocity, stress) at inlet boundary under the driven force feedback technique. The approximate value will be estimated and return the values back to the next vertical nodes as below demonstration workflow.

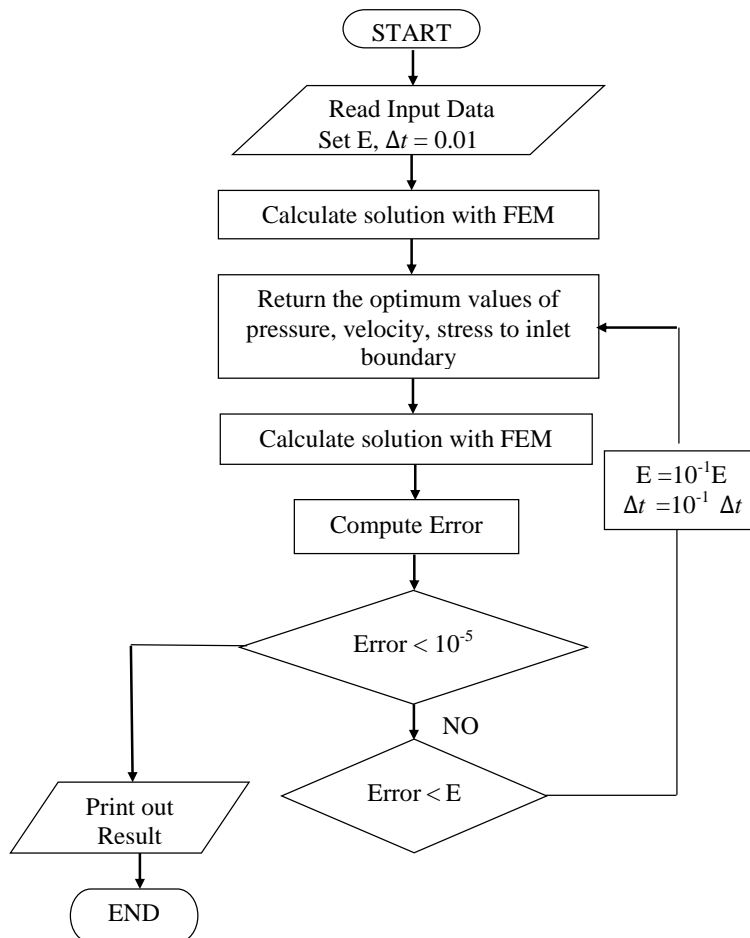


Fig. A. Flow chart of feedback of force-driven velocity flow.